Exp.-Nr. **A2-05/09**
Eingang: 15.05.2009
an PAC: 18.05.2009

Mainz Microtron MAMI

Collaboration A2: "Tagged Photons"
Spokesperson: A. Thomas

Proposal for an Experiment

"Photoproduction of Neutral Kaons on Deuterium"

Spokespersons for the Experiment:
D. M. Manley (Kent State University)
W. J. Briscoe (The George Washington University)
A. Starostin (UCLA)

Abstract of Physics:

The main objective of this proposal is to measure $d\sigma/d\Omega$ and the recoil Λ polarization P for the reaction $\gamma n \to K^0\Lambda$ using a liquid deuterium target. These measurements can be carried out using unpolarized (or circularly polarized) beam and an unpolarized target. Simultaneously we will measure $d\sigma/d\Omega$ for $\gamma p \to K^0\Sigma^+$, which will provide a check of systematics since the latter reaction has been measured previously by other groups using both liquid hydrogen and liquid deuterium targets. These measurements will provide both the GW Data Analysis Center (SAID) and the Mainz MAID Group with new data to be included in their analyses.

Abstract of Equipment:

The experiment will be performed at the tagged photon facility of MAMI. We will make use of the almost 4π coverage of the Crystal Ball and TAPS for photons, the upgraded Glasgow photon tagger, and an LD_2 target that are available with MAMI-C.

MAMI Specifications:

beam energy	1558 MeV
beam current	< 20 nA
beam polarization	unpolarized

Photon Beam Specifications:

tagged energy range	900 - 1480 MeV
photon beam polarization	unpolarized, circularly polarized

Equipment Specifications:

detectors	Crystal Ball/TAPS
target	5 cm liquid deuterium

Beam Time Request:

set–up/tests with beam	24 hours (parallel with proposal A2/ ???)
data taking	400 hours (parallel with proposal A2/ ???)

List of participating authors:

- **Institut für Physik, University of Basel, Switzerland**
  I. Jaegle, I. Keshelashvili, B. Krusche, Y. Maghrbi, F. Pheron, T. Rostomyan, D. Werthmüller
- **Institut für Experimentalphysik, University of Bochum, Germany**
  W. Meyer, G. Reicherz
- **Helmholtz–Institut für Strahlen- und Kernphysik, University of Bonn, Germany**
  R. Beck, A. Nikolaev
- **Massachusetts Institute of Technology , Cambridge, USA**
  A. Bernstein, W. Deconinck
- **JINR, Dubna, Russia**
  N. Borisov, A. Lazarev, A. Neganov, Yu.A. Usov
- **School of Physics, University of Edinburgh, UK**
  D. Branford, D.I. Glazier, T. Jude, M. Sikora, D.P. Watts
- **Petersburg Nuclear Physics Institute, Gatchina, Russia**
  V. Bekrenev, S. Kruglov, A. Koulbardis
- **Department of Physics and Astronomy, University of Glasgow, UK**
  J.R.M. Annand, D. Hamilton, D. Howdle, K. Livingston, J. Mancell, J.C. McGeorge, I.J.D. MacGregor, E.F. McNicoll, R.O. Owens, J. Robinson, G. Rosner
- **Department of Astronomy and Physics, Saint Mary's University Halifax, Canada**
  A.J. Sarty
- **Kent State University, Kent, USA**
  D.M. Manley
- **University of California, Los Angeles, USA**
  B.M.K. Nefkens, S. Prakhov, A. Starostin, I.M. Suarez
- **MAX-lab, University of Lund, Sweden**
  L. Isaksson
- **Institut für Kernphysik, University of Mainz, Germany**
  P. Aguar-Bartolome, H.J. Arends, S. Bender, A. Denig, E.J. Downie, N. Frömmgen, E. Heid, O. Jahn, H. Ortega, M. Ostrick, B.Oussena, P.B. Otte, S. Schumann, A. Thomas, M. Unverzagt
- **Institut für Physik, University of Mainz, D**
  J.Krimmer, W.Heil
- **University of Massachusetts, Amherst, USA**
  P.Martel, R.Miskimen
- **Institute for Nuclear Research, Moscow, Russia**
  G. Gurevic, R. Kondratiev, V. Lisin, A. Polonski
- **Lebedev Physical Institute, Moscow, Russia**
  S.N. Cherepnya, L.V. Fil kov, V.L. Kashevarov
- **INFN Sezione di Pavia, Pavia, Italy**
  A. Braghieri, A. Mushkarenkov, P. Pedroni
- **Department of Physics, University of Regina, Canada**
  G.M. Huber
- **Mount Allison University, Sackville, Canada**
  D. Hornidge

- **Tomsk Polytechnic University, Tomsk, Russia**
  A. Fix
- **Physikalisches Institut, University of Tübingen, Germany**
  P. Grabmayr, T. Hehl, D.G. Middleton
- **George Washington University, Washington, USA**
  W. Briscoe, T. Morrison, B.Oussena, B. Taddesse, M. Taragin
- **Catholic University, Washington, USA**
  D. Sober
- **Rudjer Boskovic Institute, Zagreb, Croatia**
  M. Korolija, D. Mekterovic, S. Micanovic, I. Supek

1 Introduction

1.1 Motivation

Strangeness photoproduction is a fundamental process and an important tool for gaining insight into nucleon resonances. There are six elementary strangeness photoproduction reactions:
(1) $\gamma + p \to K^+ + \Lambda$;
(2) $\gamma + p \to K^+ + \Sigma^0$;
(3) $\gamma + p \to K^0 + \Sigma^+$;
(4) $\gamma + n \to K^0 + \Lambda$;
(5) $\gamma + n \to K^0 + \Sigma^0$;
(6) $\gamma + n \to K^+ + \Sigma^-$.
Among these reactions, (1) and (2) have received intensive experimental attention [1, 2, 3, 4]. Our proposal will focus on reaction (4), which has an all-neutral final state and has received little experimental attention [5]. This reaction is ideally suited to a detailed study with the Crystal Ball-TAPS set-up at MAMI-C. Not only is this reaction of interest in itself, but also it is required to understand hypernuclear production by the electromagnetic interaction. Kaon photoproduction on the neutron is isospin-1/2 selective and may provide essentially new information about the spectrum of N^* resonances. We should also be able to determine the recoil Λ polarization P, since the Λ is self-analyzing.
A variety of reasons leads us to believe that the photoproduction of the $K^0\Lambda$ system should have significant contributions from N^* production in the near-threshold region. This expectation is in accord with a unitary coupled-channels analysis of hadronic and electromagnetic $K\Lambda$ production [6] that found appreciable branching ratios of 10-20% of the $S_{11}(1650)$ and $P_{11}(1710)$ states into the $K\Lambda$ channel. Significant $K\Lambda$ couplings for these states are also predicted by a relatived quark-model calculation [7]. Furthermore, a relativized quark-model calculation [8] predicts $P_{11}(1710)$ to have helicity photocouplings that are about equal in magnitude but opposite in sign for γn and γp.
The integrated cross section for $\pi^- p \to K^0\Lambda$ is shown in Fig. 1. A strong peak occurs at a c.m. energy W of about 1.7 GeV, which is arguably associated with the $P_{11}(1710)$ resonance. The data of Jones *et al.* [9] (filled diamonds) suggest that this peak might have a relatively narrow width (about 70 MeV), but better data are needed at energies above the peak to confirm this. This suggestive structure is of particular interest in view of recent claims for a narrow resonance in $\gamma n \to \eta n$ at 1685 MeV [10, 11].
The quality of the data shown in Fig. 1 make it clear why little is known experimentally about resonances that decay to $K\Lambda$. The $P_{11}(1710)$ is of special interest. This resonance, although given a rating of 3 stars by the Particle Data Group (PDG) [12], is little understood. It is known to have a small πN branching ratio, which makes it very difficult to study in traditional elastic πN scattering experiments. Even the total decay width of this state is not well known (the PDG estimate is 50 to 250 MeV). It is commonly believed that the $P_{11}(1710)$ has a significant branching ratio to $K\Lambda$; thus, $K\Lambda$ photoproduction at MAMI-C might shine new light on the properties of this state.
Interestly, two entirely different experiments recently revealed evidence for narrow structures at a c.m. energy of about 1.7 GeV. (1) In an experiment at JLab, the CLAS Collaboration measured the cross section for $ep \to e'p\pi^+\pi^-$ and observed a narrow resonant structure with a mass of about 1.7 GeV, which was best described as a P_{13} state [19]. (2) In an experiment at GRAAL, a narrow resonance-like structure was seen for the reaction $\gamma n \to \eta n$ at about 1.7 GeV, which was not observed in measurements on the proton [10]. Clearly, further study of other resonance regions in the vicinity of 1.7 GeV is warranted.

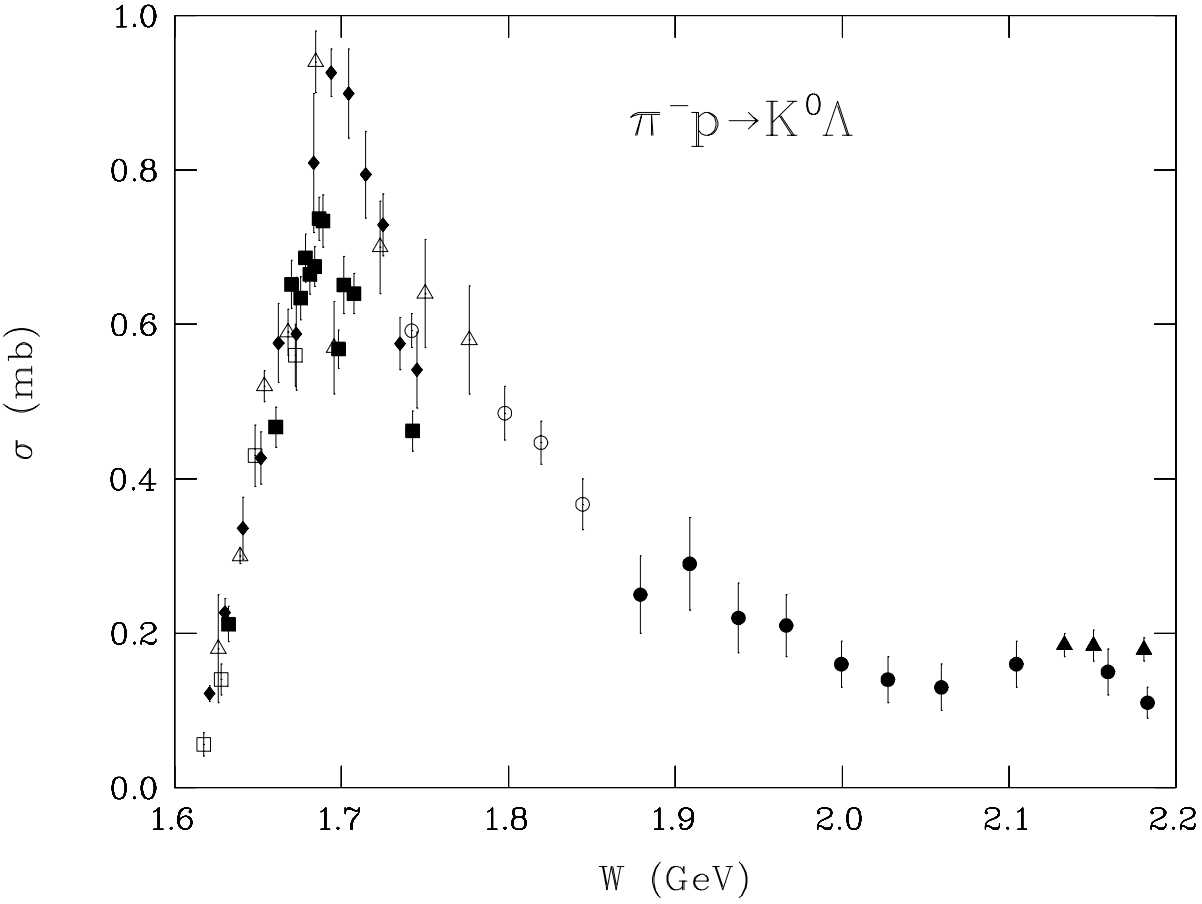

Figure 1: Integrated cross section for $\pi^- p \to K^0\Lambda$ as a function of total c.m. energy W. Data from Bertanza *et al.* [13] are shown as open squares, from Knasel *et al.* [14] as filled squares, from Binford *et al.* [15] as open circles, from Saxon *et al.* [16] as filled circles, from Van Dyke *et al.* [17] as open triangles, from Dahl *et al.* [18] as filled triangles, and from Jones *et al.* [9] as filled diamonds.

1.2 Theoretical Considerations

A wide variety of theoretical models have been proposed to describe the elementary kaon photoproduction processes but no one model explains all measured observables. The $\gamma n \to K^0\Lambda$ reaction is expected to help clarify the strangeness photoproduction mechanism because of the following features:

1. In contrast to $\gamma p \to K^+\Lambda$, the Born term in the t channel does not contribute to $\gamma n \to K^0\Lambda$ because no charge is involved.

2. The strong coupling constants in the u channel for Σ^0 and other isovector exchanges have the same value but are of opposite sign to those in $\gamma p \to K^+\Lambda$ because of isospin symmetry.

3. The electromagnetic coupling constants of resonances in the s channel, *e.g.*, $g_{N^*n\gamma}$, and in the t channel, *e.g.*, $g_{K^*K^0\gamma}$, are different from those in $\gamma p \to K^+\Lambda$.

Figure 2 shows recent isobar-model results for the angular distributions and cross sections of reactions (1) and (4) at $E_\gamma = 1.05$ GeV. Solid and dashed curves show predictions for two different parameter sets. Both parameter sets give similar results for $\gamma p \to K^+\Lambda$ but the predicted angular

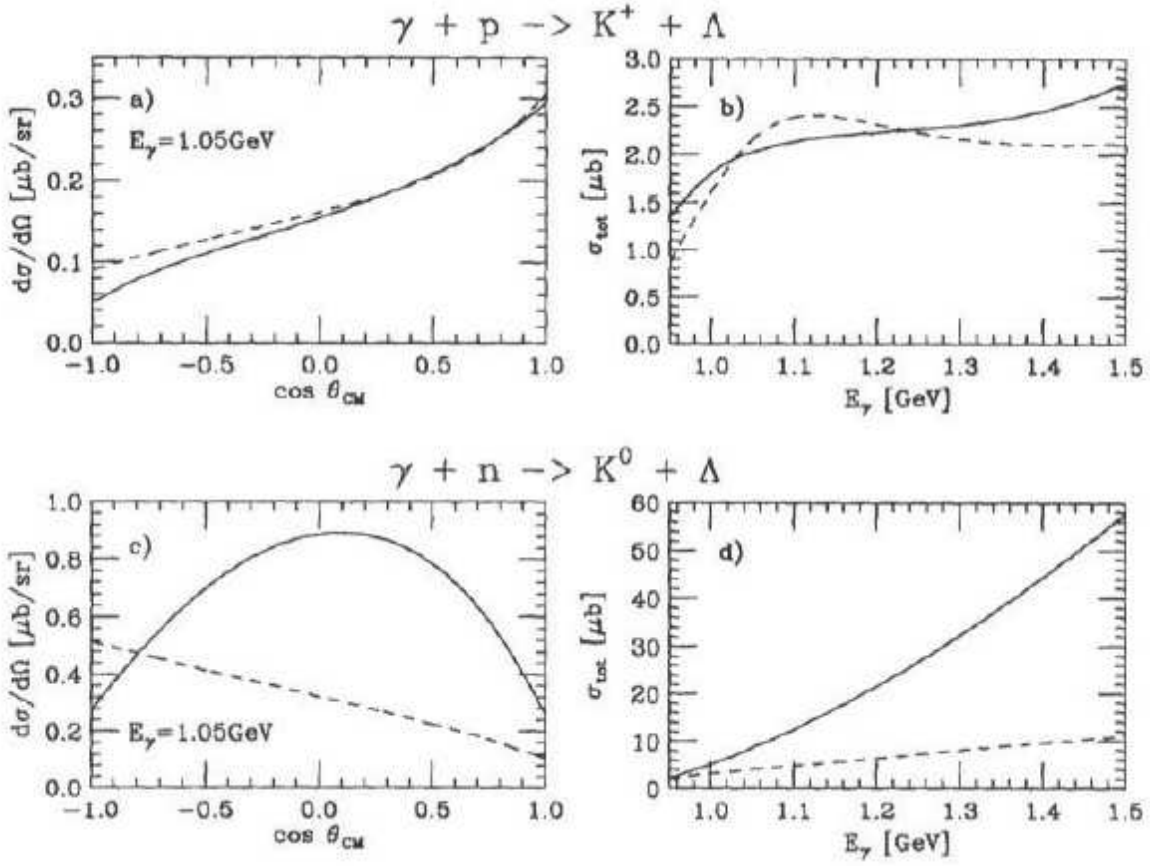

Figure 2: The angular distribution of K^+ (K^0) Λ photoproduction process on the nucleon at E_γ = 1.05 GeV (a) and c)). Solid and dashed curves show the results from the parameters sets of Ref. [23] and [24], respectively. Figures b) and d) show total cross sections for each production channel.

distributions are very different for $\gamma n \to K^0\Lambda$. Figure 3 similarly shows different isobar-model predictions for the $\gamma n \to K^0\Lambda$ reaction. The particular models referred to in the figure are Saclay-Lyon (SLA) [20], Kaon-MAID (K-MAID) [21], and M2 and H2 [22]. These models also reveal more different results for $\gamma n \to K^0\Lambda$ reaction than for $\gamma p \to K^+\Lambda$. Figure 3 demonstrates that the K-MAID and SLA models are much more sensitive to a contribution from K_1 exchange than the M2 or H2 models. This phenomenon is valid for photon energies up to 1.5 GeV and kaon lab angles up to 50° [22]. Measurement of the $K^0\Lambda$ channel is therefore very important to give new information on strangeness production by the electromagnetic interaction.

1.3 Prior measurements

Only very recently have there been any experimental investigations of $\gamma n \to K^0\Lambda$. In Fall 2006, the first part of the g13 experiment using tagged photons with circular polarization was completed in Hall B at JLab [25]. The data were taken with E_γ of 0.4-1.9 GeV and 0.5-2.5 GeV. As yet, no results from the analysis of these data have been published. In view of the now well-known disagreement between measurements of $\gamma p \to K^+\Lambda$ obtained by the CLAS Collaboration [1] with previous data from SAPHIR at Bonn [4], it is clear that independent measurements for $\gamma n \to K^0\Lambda$ are warranted.

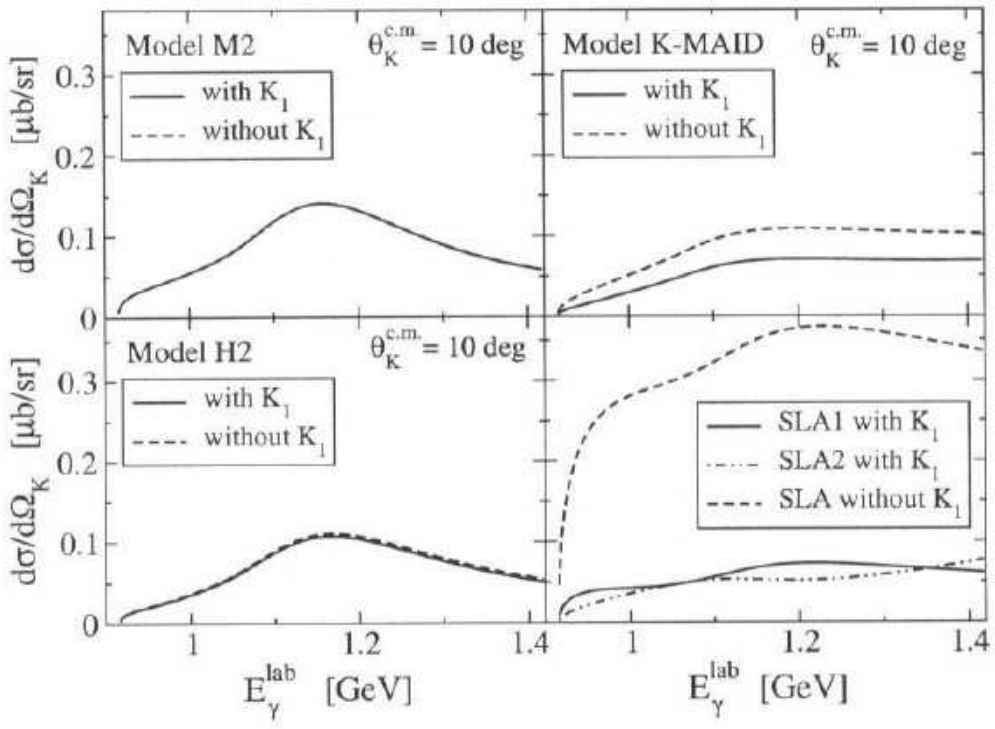

Figure 3: Contribution of the K_1 exchange to the differential cross section in $\gamma n \to K^0\Lambda$ is shown as a function of energy at kaon angle of 10°.

In 2007, Watanabe *et al.* [26] reported the first measurement of the quasifree photoproduction of neutral kaons on a ^{12}C target in the threshold region ($E_\gamma = 0.8$–1.1 GeV). The experiment was performed using the tagged photon beam facility at the Laboratory of Nuclear Science (LNS) at Tohoku University in Sendai, Japan. Momentum spectra as well as integrated cross sections were obtained. K^0 angular distributions could not be directly obtained from these data due to the limited kinematical acceptance.
In 2008, Tsukada *et al.* [5] reported the first measurement of K^0 photoproduction on a deuterium target. These measurements were conducted in the threshold region ($E_\gamma = 0.8$–1.1 GeV) at the LNS of Tohoku University. Inclusive momentum distributions were obtained and compared with theoretical calculations. The measured momentum spectra differed considerably in shape from those calculated with Kaon-MAID [21] and it was found that Kaon-MAID gives larger cross sections than the measured spectra. While angular distributions were not extracted, comparison of the momentum spectra with model predictions suggested than an enhancement of the elementary $\gamma n \to K^0\Lambda$ angular distribution in the backward direction was needed to explain the measured shape of the K^0 momentum spectrum.

2 Experimental issues

The threshold for $\gamma n \to K^0\Lambda$ occurs at an incident photon energy $E_\gamma = 915.3$ MeV, corresponding to a c.m. energy of $W = 1613.3$ MeV. With MAMI-C, we should be able to measure data with reasonable statistics up to $E_\gamma = 1400$ MeV, corresponding to a c.m. energy of about 1875 MeV (*i.e.*, full coverage of the "second resonance region").
We measured data for this reaction from two separate test runs at MAMI-C. The first run

occurred in May 2007 during a period in which both hydrogen and deuterium measurements were taken with unpolarized beam. The second run occurred in December 2007 when we had about two weeks of unpolarized beam measurements with a 5-cm liquid deuterium target. Not all the data obtained during these test runs were usable for our analysis since we require a high multiplicity trigger ($M \geq 2$) and the maximum beam energy.

2.1 Kinematic Fitting and Comparisons with Monte Carlo Simulations

Our analysis for $\gamma n \to K^0\Lambda$ is very similar to that used by the SAPHIR Collaboration in their analysis of $\gamma p \to K^0\Sigma^+$ [3]. We identify the reaction $\gamma n \to K^0\Lambda$ by its neutral decay channel:

$$\gamma n \to K^0\Lambda \to (\pi^0\pi^0)(\pi^0 n) \to 6\gamma n.$$

That is, we begin by selecting events involving exactly six "clusters" within the Crystal Ball. Because the threshold for detecting neutrons is relatively low and because we are measuring this reaction at low energies when most of the neutrons go forward through the beam pipe opening for the Crystal Ball, we assume that the clusters of deposited energy in the Crystal Ball are due to photons. The technique of kinematic fitting is being used to analyze the data. Figure 4 is a plot of the Z-vertex distribution for the primary interaction of $\gamma n \to K^0\Lambda$ events in the target. The comparison with Monte Carlo (MC) simulated events is excellent. (Note that all results shown in this proposal are *preliminary* as our analysis procedures are still being refined.) Since the neutral kaon and Λ are not produced at rest, and because the K^0_S and Λ decay weakly, they propagate away from the primary vertex before they decay. Kinematic fitting is necessary in order to calculate their secondary vertices for the locations where they decay in the Crystal Ball. Each 6-cluster event is tested for five possible hypotheses:

- that the event is from $\gamma n \to K^0\Lambda$;
- that the event is from $\gamma p \to K^0\Sigma^+$, where the Σ^+ is identified from its weak decay $\Sigma^+ \to \pi^0 p$;
- that the event is from $\gamma n \to K^0\Sigma^0$ (most of these events produce 7-cluster events which are immediately excluded from further analysis);
- that the event is from $\gamma N \to \eta N$; and
- that the event is from $\gamma N \to 3\pi^0 N$, where the final-state pions are assumed to be produced at the primary vertex.

Events selected as coming from the reaction $\gamma n \to K^0\Lambda$ are required to have the highest likelihood out of these hypotheses. The angle-averaged detection efficiency for $\gamma n \to K^0\Lambda$ events using this criterion is about 25% over almost our entire energy range (See Fig. 5). Figure 6 shows the confidence level (CL) of events identified as coming from $\gamma n \to K^0\Lambda$. We have not imposed a CL cut for any of the figures presented in this proposal. Our plan is to impose a cut that the final selected events must have CL$>$0.15, which will lead to a much cleaner event sample but will decrease the average acceptance to about 17%. The relative survival contributions of the primary background reactions were estimated using Monte Carlo generated events. For each generated background event, those that survived the selection tests for $\gamma n \to K^0\Lambda$ events were counted as background. The average results given as percentages with respect to the generated background events are summarized in Table I.
In order to estimate and subtract background contributions, MC data for each of these hypotheses were simulated and analyzed using the same criteria as for the real data. The backgrounds from direct $3\pi^0$ and η production are strongly suppressed within our analysis, with the main

Table 1: Background contributions calculated from Monte Carlo simulated events.

Reaction	Relative Survival Contribution (%)
$\gamma p \to K^0\Sigma^+$	2.15
$\gamma n \to K^0\Sigma^0$	0.76
$\gamma N \to \eta N$	0.38
$\gamma N \to 3\pi^0 N$	1.02

background to $\gamma n \to K^0\Lambda$ coming from $\gamma p \to K^0\Sigma^+$ events. Details of the event selection criteria are summarized below:

1) We require that the invariant mass of four of the photon clusters is consistent with the mass of the K^0_S meson and that their corresponding missing mass is consistent with the mass of the Λ hyperon. Figures 7 and 8, respectively, show the distributions of invariant mass and missing mass for the 4-photons identified as coming from the decay $K^0_S \to 2\pi^0 \to 4\gamma$.
2) For the four photons identified as coming from the decay of a K^0_S meson, we require that we can reconstruct the two neutral pions coming from the decay $K^0_S \to 2\pi^0 \to 4\gamma$. Figure 9 shows the distribution of invariant mass for the photon pairs identified as being produced from these π^0 decays.
3) For the two photons identified as coming from the decay of a Λ hyperon, we require that their invariant mass is consistent with that of a π^0 and that their missing mass is consistent with that of a neutron. Figure 10 shows the distribution of missing mass from the six photon clusters identified as coming from the chain $\gamma n \to K^0_S\Lambda \to 3\pi^0 n \to 6\gamma n$.
With a high multiplicity trigger ($M \geq 2$) and the CB + TAPS set-up, we simultaneously measure events for the reaction $\gamma p \to K^0\Sigma^+$. In our analysis of $\gamma n \to K^0\Lambda$, we are carrying out a parallel analysis of data for the reaction $\gamma p \to K^0\Sigma^+$, which we identify by its neutral decay channel:

$$\gamma p \to K^0\Sigma^+ \to (\pi^0\pi^0)(\pi^0 p) \to 6\gamma p.$$

Events selected as coming from the reaction $\gamma p \to K^0\Sigma^+$ are required to have the highest likelihood out of the same hypotheses used to select $\gamma n \to K^0\Lambda$ events. The angle-averaged acceptance for $\gamma p \to K^0\Sigma^+$ events using this criterion is about 4% over almost our entire energy range. Since cross-section data are available in the literature [27] for this reaction, we will be able to compare our results with previous measurements. Consequently, we can use this comparison to check our technique for analyzing $\gamma n \to K^0\Lambda$ events. Figure 11 shows the experimental distribution of missing mass from the four photon clusters identified as coming from the chain $\gamma p \to K^0\Sigma^+$ followed by $K^0_S \to 2\pi^0 \to 4\gamma$. A comparison of our preliminary results for $\sigma(\gamma p \to K^0\Sigma^+)$ with prior measurements is shown in Fig. 12. The agreement is very encouraging and provides further support for our analysis methods.

3 Event rates and beamtime estimate

For the measurement of the differential cross sections we aim at a statistical precision of 3% assuming 10 bins of $\cos\theta$ and a 20-MeV binning of incident photon energies (corresponding to approximately 10-MeV binning in W). The necessary beam time is given by

$$\Delta t = [\delta^2_{\rm stat} \cdot \Delta\sigma_0 \cdot N_\gamma \cdot N_t \cdot \epsilon \cdot b_K \cdot b_\Lambda]^{-1} \ ,$$

with the following notation:

- δ_{stat}: relative statistical uncertainty $\Rightarrow 0.03$
- N_γ: number of photons per 20-MeV incident photon energy $\Rightarrow 5 \times 10^6$ s^{-1}
- N_t: surface density of target nuclei (5-cm liquid deuterium target) $\Rightarrow 0.25$ b^{-1}
- ϵ: detection efficiency, calculated from MC simulation (with CL cut) as $\Rightarrow 0.17$
- b_K: decay branching ratio of $K^0 \to K^0_S \to 2\pi^0 \to 4\gamma \Rightarrow 0.5 \times 0.30 = 0.15$
- b_Λ: decay branching ratio of $\Lambda \to \pi^0 n \to 2\gamma n \Rightarrow 0.36$
- $\Delta\sigma_0$: unpolarized cross section in the respective angular bins.
  We assume minimal $\Rightarrow 0.1$ μb

With these numbers we arrive at a beam time estimate of 300 hours.
We request an additional 100 hours of running with empty target for background subtraction.
Our total requested beamtime is therefore

400 hours.

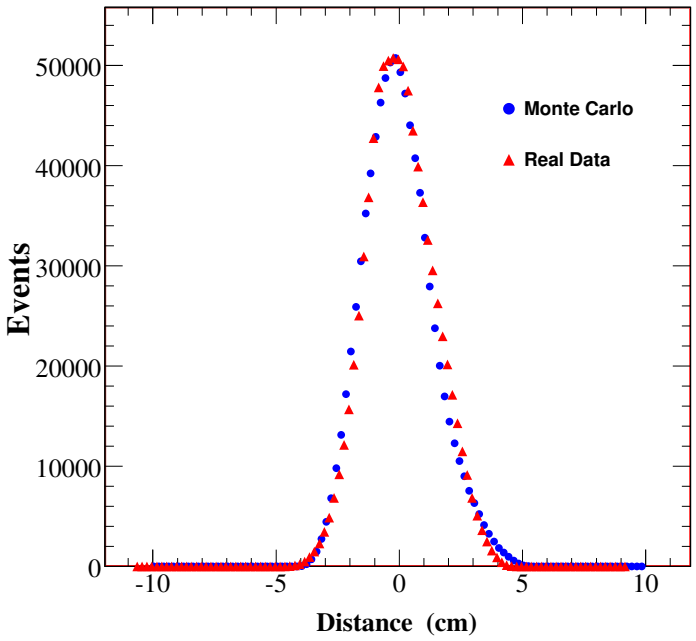

Figure 4: The experimental Z-vertex distribution for $\gamma n \to K^0\Lambda$ events compared with results from a Monte Carlo simulation.

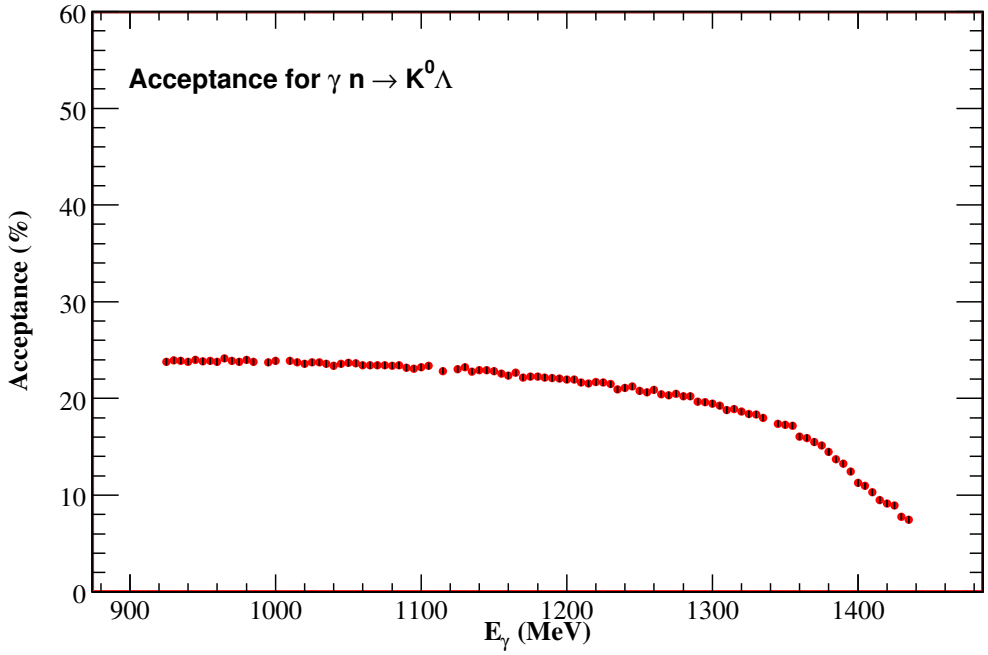

Figure 5: The angle-averaged acceptance for detecting $\gamma n \to K^0\Lambda$ events as a function of incident photon energy.

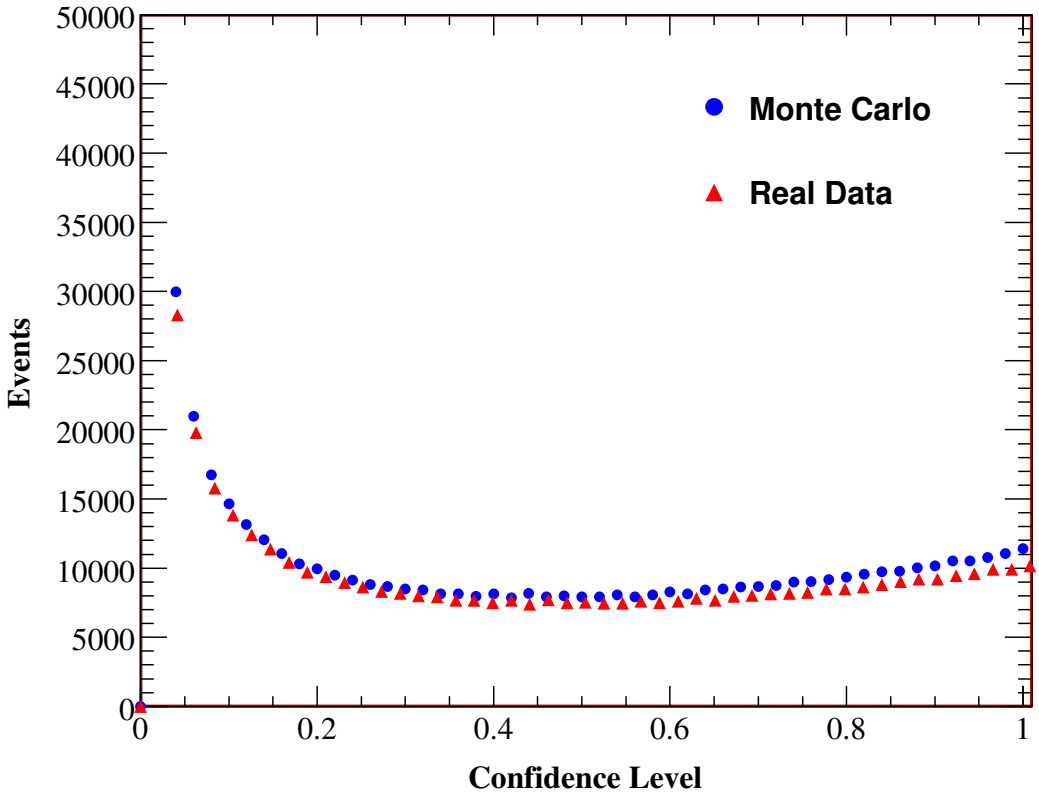

Figure 6: Confidence level for events identified as from $\gamma n \to K^0\Lambda$.

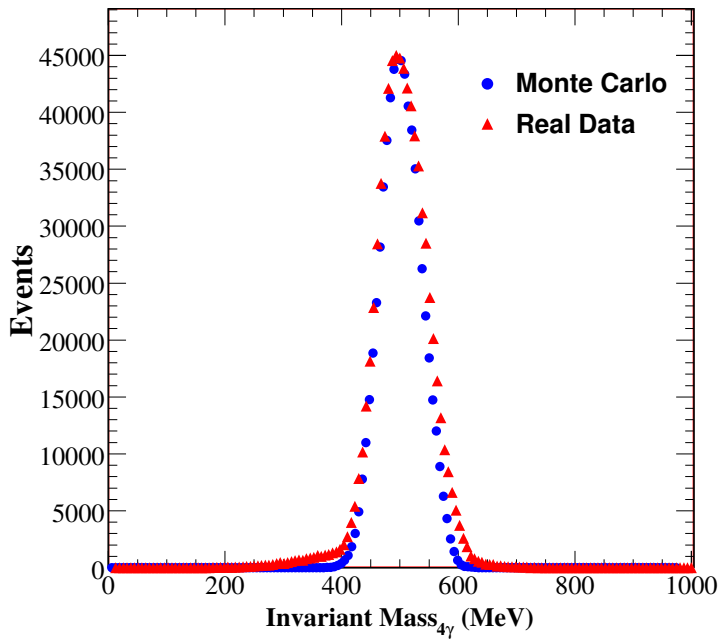

Figure 7: The distribution of invariant mass for the four photon clusters identified as coming from $\gamma n \to K^0\Lambda$ followed by $K^0_S \to 2\pi^0 \to 4\gamma$. The peak is near the mass (497.6 MeV) of the neutral kaon.

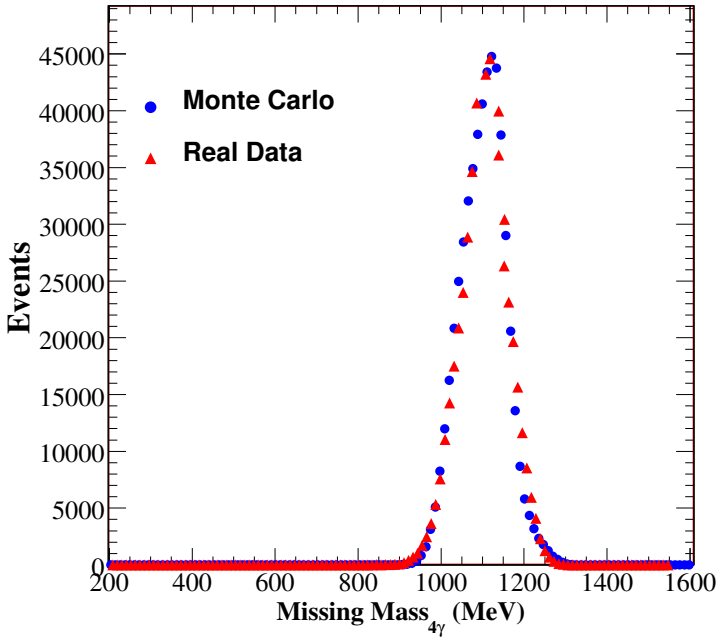

Figure 8: The distribution of missing mass for the four photon clusters identified as coming from $\gamma n \to K^0\Lambda$ followed by $K^0_S \to 2\pi^0 \to 4\gamma$. The peak is near the mass (1115.7 MeV) of the Λ hyperon.

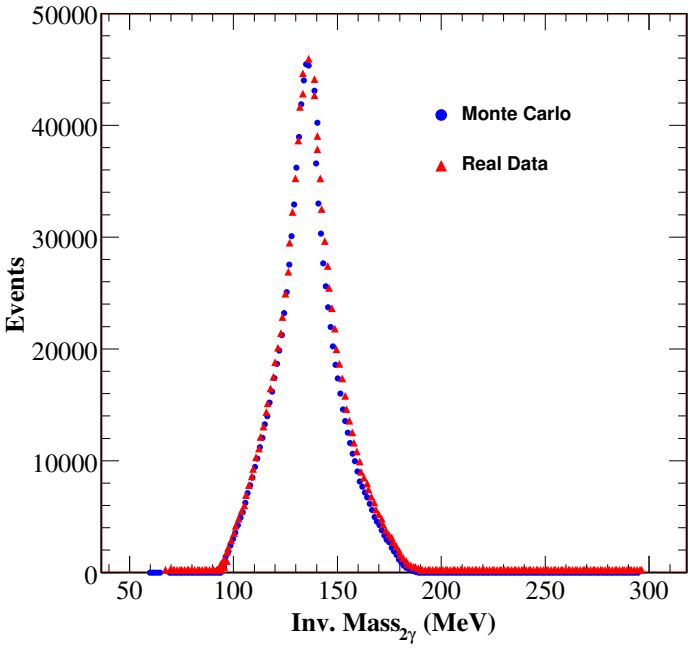

Figure 9: The distribution of invariant mass for the two photon clusters identified as coming from $K_S^0 \to 2\pi^0$ followed by $\pi^0 \to 2\gamma$. The peak is near the mass (135.0 MeV) of the neutral pion.

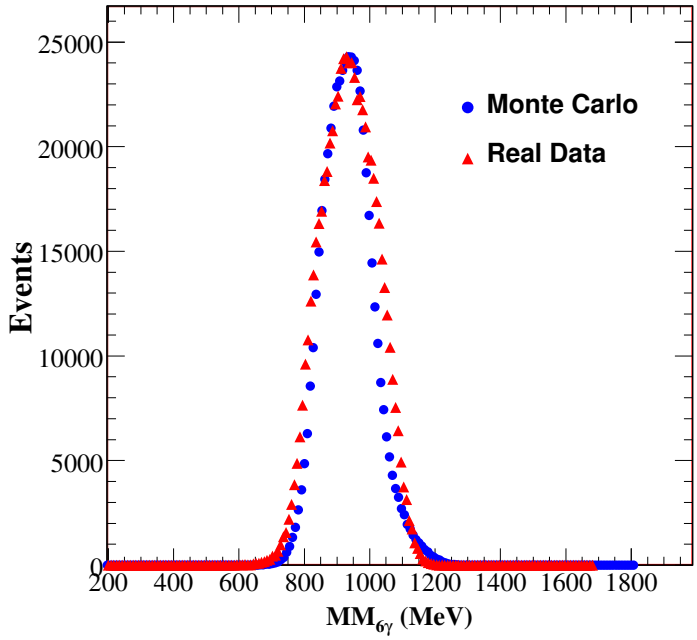

Figure 10: The distribution of missing mass for the six photon clusters identified as coming from the chain $\gamma n \to K_S^0 \Lambda \to 3\pi^0 n \to 6\gamma n$. The peak is near the mass (939.6 MeV) of the neutron.

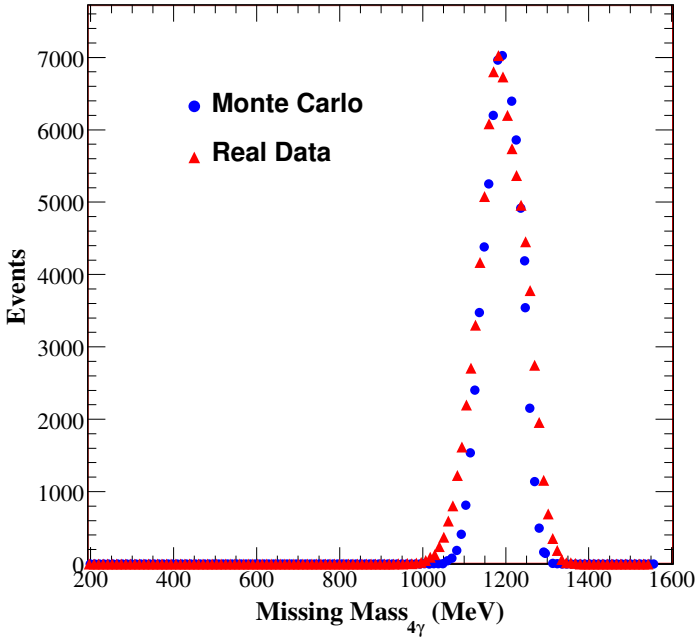

Figure 11: The distribution of missing mass for the four photon clusters identified as coming from $\gamma p \rightarrow K^0\Sigma^+$ followed by $K^0_S \rightarrow 2\pi^0 \rightarrow 4\gamma$. The peak is near the mass (1189.4 MeV) of the Σ^+ hyperon.

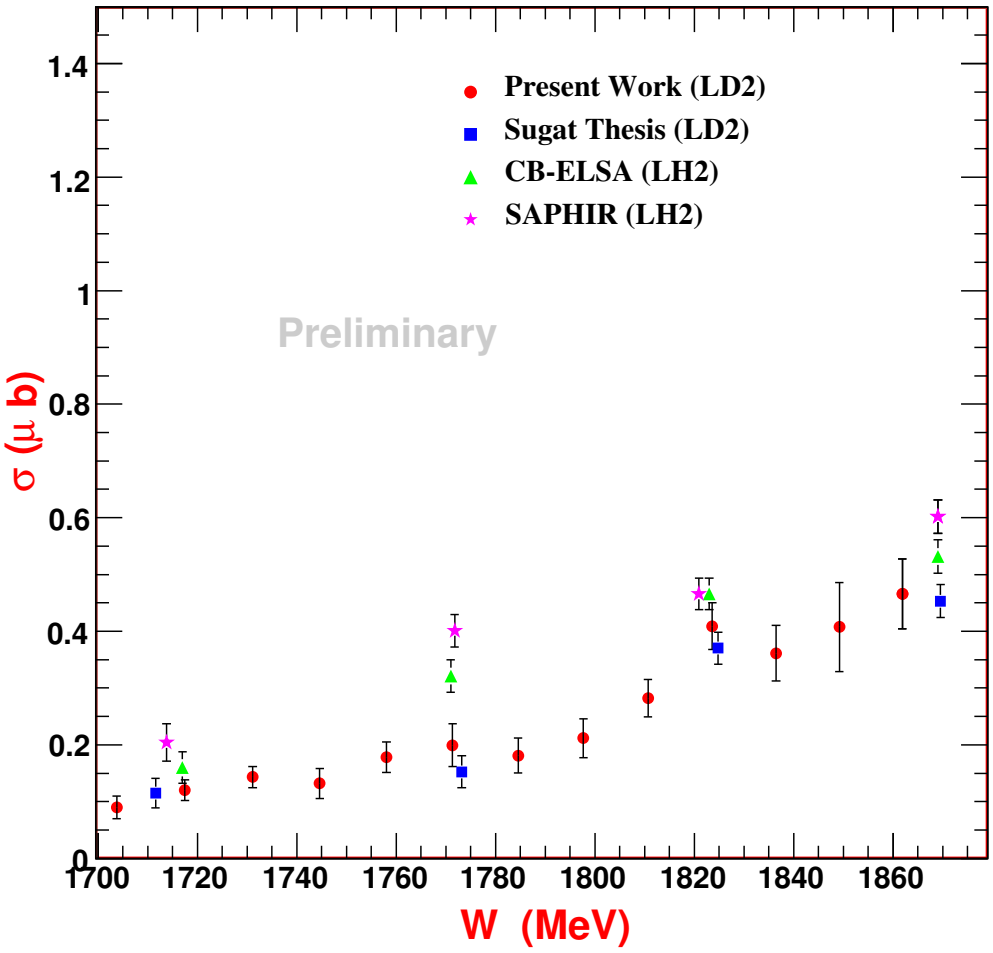

Figure 12: Comparison of our preliminary results (filled red circles) for $\sigma(\gamma p \to K^0\Sigma^+)$ with prior measurements: blue squares [28], green triangles [27], pink stars [29].

A Experimental apparatus

A.1 Photon Beam

The A2 photon beam is derived from the production of Bremsstrahlung photons during the passage of the MAMI electron beam through a thin radiator. The resulting photons can be circularly polarized, with the application of a polarized electron beam, or linearly polarized, in the case of a crystalline radiator. The degree of polarization achieved is dependent on the energy of the incident photon beam (E_0) and the energy range of interest, but currently peaks at ~75% for linear polarization (Fig. 13) and ~85% for circular polarization (Fig. 14). The maximum degree of linear polarization should be further improved by 5 to 10% by the end of 2009 when the collimation and beam monitoring systems will be optimised for MAMI-C during the installation of the Frozen Spin Target. The Glasgow Photon Tagger (Fig. 15) provides energy tagging of the photons by detecting the post-radiating electrons and can determine the photon energy with a resolution of 2 to 4 MeV depending on the incident beam energy, with a single-counter time resolution $\sigma_t = 0.117\,\text{ns}$ [30]. Each counter can operate reliably to a rate of ~1 MHz, giving a photon flux of $2.5 \cdot 10^5$ photons per MeV. Photons can be tagged in the momentum range from 4.7 to 93.0% of E_0.

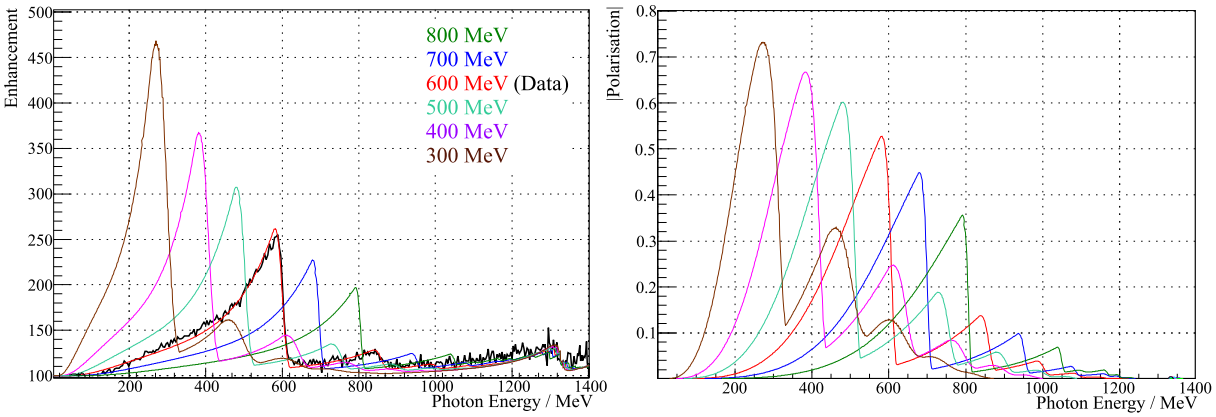

Figure 13: Linear polarization available with the current collimation system for a variety of crystal orientations. The thin black lines are data obtained during recent MAMI-C runs.

To augment the standard focal plane detector system and make use of the Tagger's intrinsic energy resolution of 0.4 MeV (FWHM), there exists a scintillating fiber detector ('Tagger Microscope') that can improve the energy resolution by a factor of about 6 for a ~100 MeV wide region of the focal plane (dependent on its position) [31].

A.2 Frozen-Spin Target

Polarization experiments using high density solid-state targets in combination with tagged photon beams can reach the highest luminosities. For the double polarization measurements planned with the Crystal Ball detector on polarized protons and deuterons a specially designed, large horizontal ^{3}He/^{4}He dilution refrigerator was built in cooperation with the Joint Institute for Nuclear Research (JINR) Dubna (see Fig. 16). It has minimum limitations for the particle detection and fits into the central core of the inner Particle Identification Detector (PID2). This was achieved by using the frozen spin technique with the new concept of placing a thin superconducting holding coil inside the polarization refrigerator. Longitudinal and transverse polarizations will be possible.
Highest nucleon polarization in solid-state target materials is obtained by a microwave pumping

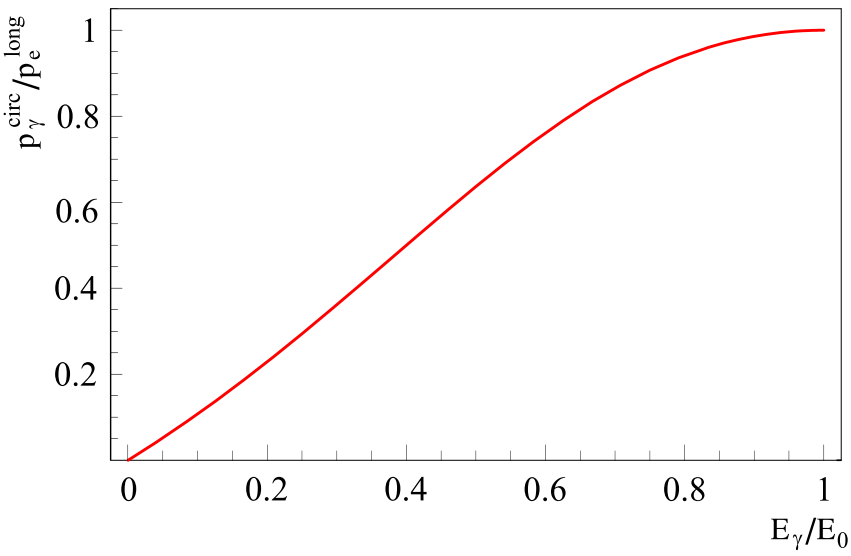

Figure 14: Helicity transfer from the electron to the photon beam as function of the energy transfer. The MAMI beam polarization is $P_e \approx 85\%$.

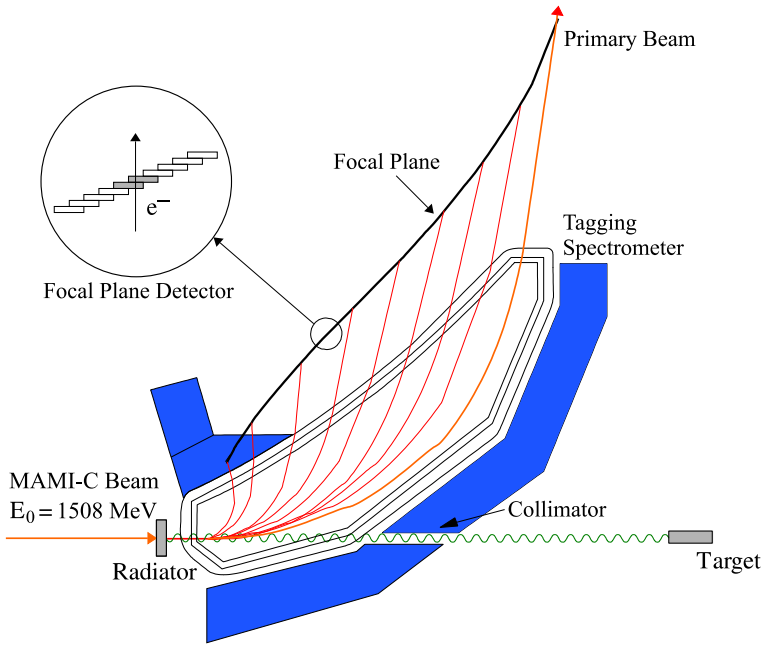

Figure 15: The Glasgow photon tagging spectrometer.

Figure 16: The new dilution refrigerator for the Crystal Ball Frozen Spin Target.

process, known as 'Dynamic Nucleon Polarization' (DNP). This process is applicable to any nucleus with spin and has already been used in different experiments with polarized proton and deuteron targets. The geometric configuration of the target is the same for the polarized proton and neutron setup. However, since the polarization measurement of the deuteron is more delicate due to the small size of the polarization signals, the modification of some basic components is needed. The reason for this is twofold: firstly the magnetic moment of the deuteron is smaller than that of the proton and, in addition, the interaction of the deuteron quadrupole moment with the electric field gradient in the sample broadens the deuteron polarization signal. An accuracy $\delta P_p/P_p$ of 2 to 3% for the protons and $\delta P_D/P_D$ of 4 to 5% for the deuterons is expected in the polarization measurement. It has also to be taken into account that the measured deuteron polarization P_D is not equal to the neutron polarization P_n. Assuming a 6% admixture of the D-state of the deuteron, a calculation based on the Clebsch-Gordon coefficients leads to $P_n = 0.91\ P_D$. Several polarized proton and deuteron materials are available such as alcohols and deuterated alcohols (e.g. butanol C_4H_9OH), NH_3, ND_3 or ^{6}LiD. The most important criteria in the choice of material suitable for particle physics experiments are the degree of polarization P and the ratio k of free polarizable nucleons to the total number of nucleons. Further requirements on polarized target materials are a short polarization build-up time and a simple, reproducible target preparation. The polarization resistance against radiation damage is not an issue for experiments with a low intensity tagged photon beam ($\dot{N}_\gamma \approx 5 \cdot 10^7\ s^{-1}$) as will be used here. However, the limitations of a reduced relaxation time due to overheating of the target beads (Kapitza resistance) will have to be investigated.

Taking all properties together, butanol and deuterated butanol are the best material for this experiment. For protons we expect a maximum polarization of $P_p = 90\%$ and an average polarization of $P_p = 70\%$ in the frozen spin mode. Recently, a deuteron polarization $P_D = 80\%$

was obtained with Trityl doped butanol targets at 2.5 T magnetic field in a ^{3}He/^{4}He dilution refrigerator. At a 0.4 T holding field an average neutron polarization P_n (see above) of 50% will be obtained. The filling factor for the ∼2 mm diameter butanol spheres into the 2 cm long, 2 cm diameter target container will be around 60%. The experience from the GDH runs in 1998 [32] shows that, with a total tagged photon flux of $5 \cdot 10^7$, relaxation times of about 200 hours can be expected. The polarization has to be refreshed by microwave pumping every two days.
In conclusion, we estimate that we will achieve the following target parameters:

- Maximum total tagged photon flux in the energy range of 4.7 to 93% of E_0: $\dot{N}_\gamma \approx 5 \cdot 10^7\,\mathrm{s}^{-1}$, with relaxation time of 200 hours.
- Target proton density in 2 cm cell: $N_T \approx 9.1 \cdot 10^{22}\mathrm{cm}^{-2}$ (including dilution and filling factors)
- Average proton polarization $P_p = 70\%$
- Target deuteron density in 2 cm cell: $N_T \approx 9.4 \cdot 10^{22}\mathrm{cm}^{-2}$ (including dilution and filling factors)
- Average neutron polarization $P_n = 50\%$

A.3 Crystal Ball Detector System

The central detector system consists of the Crystal Ball calorimeter combined with a barrel of scintillation counters for particle identification and two coaxial multiwire proportional counters for charged particle tracking. This central system provides position, energy and timing information for both charged and neutral particles in the region between 21° and 159° in the polar angle (θ) and over almost the full azimuthal (ϕ) range. At forward angles, less than 21°, reaction products are detected in the TAPS forward wall. The full, almost hermetic, detector system is shown schematically in Fig. 17 and the measured two-photon invariant mass spectrum is shown in Fig. 18.
The Crystal Ball detector (CB) is a highly segmented 672-element NaI(Tl), self triggering photon spectrometer constructed at SLAC in the 1970s. Each element is a truncated triangular pyramid, 41 cm (15.7 radiation lengths) long. The Crystal Ball has an energy resolution of $\Delta E/E = 0.020 \cdot E[\mathrm{GeV}]^{0.36}$, angular resolutions of $\sigma_\theta = 2 \ldots 3°$ and $\sigma_\phi = \sigma_\theta / \sin\theta$ for electromagnetic showers [33]. The readout electronics for the Crystal Ball were completely renewed in 2003, and it now is fully equipped with SADCs which allow for the full sampling of pulse-shape element by element. In normal operation, the onboard summing capacity of these ADCs is used to enable dynamic pedestal subtraction and the provision of pedestal, signal and tail values for each element event-by-event. Each CB element is also newly equipped with multi-hit CATCH TDCs. The readout of the CB is effected in such a way as to allow for flexible triggering algorithms. There is an analogue sum of all ADCs, allowing for a total energy trigger, and also an OR of groups of 16 crystals to allow for a hit-multiplicity second-level trigger - ideal for use when searching for high multiplicity final states.
In order to distinguish between neutral and charged particles species detected by the Crystal Ball, the system is equipped with PID2, a barrel detector of 24 50 mm long, 4 mm thick scintillators, arranged so that each PID2 scintillator subtends an angle of 15° in ϕ. By matching a hit in the PID2 with a corresponding hit in the CB, it is possible to use the locus of the $\Delta E, E$ combination to identify the particle species (Fig. 19). This is primarily used for the separation of charged pions, electrons and protons. The PID2 covers from 15° to 159° in θ.
The excellent CB position resolution for photons stems from the fact that a given photon triggers several crystals and the energy-weighted mean of their positions locates the photon position to better than the crystal pitch. For charged particles which deposit their energy over only one

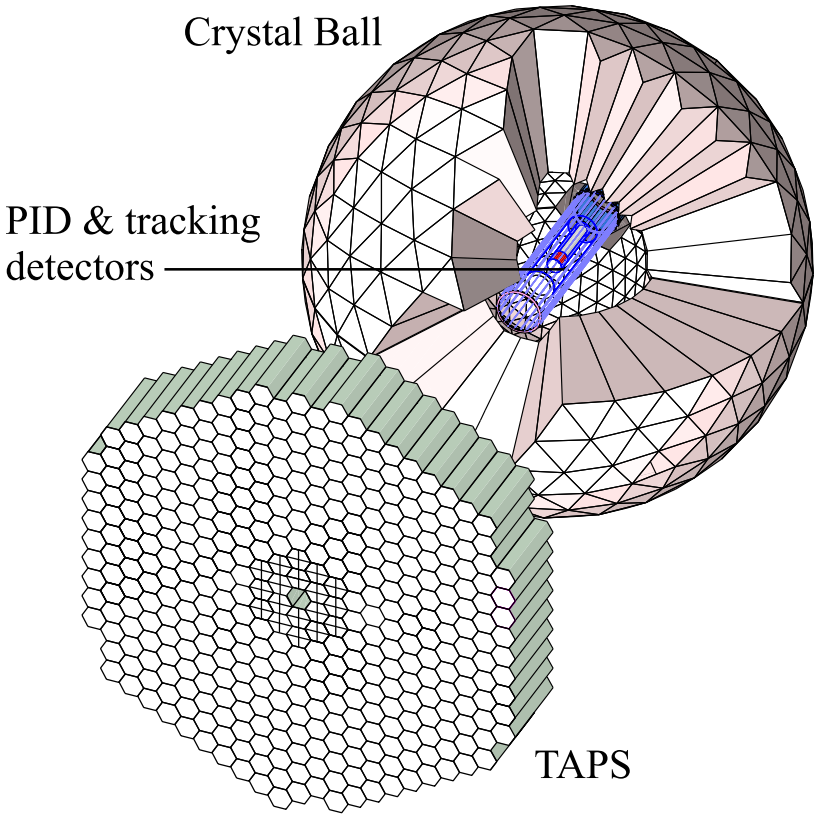

Figure 17: The A2 detector setup: The Crystal Ball calorimeter, with cut-away section showing the inner detectors, and the TAPS forward wall.

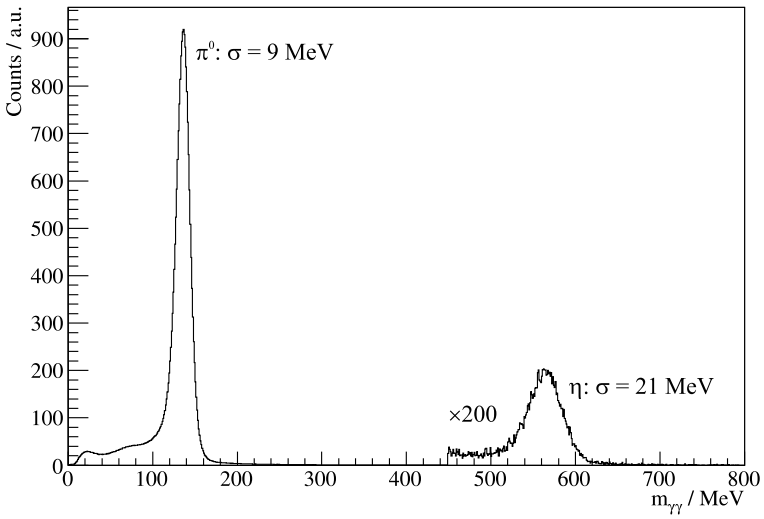

Figure 18: Two photon invariant mass spectrum for the CB/TAPS detector setup. Both η and π^0 mesons can be clearly seen.

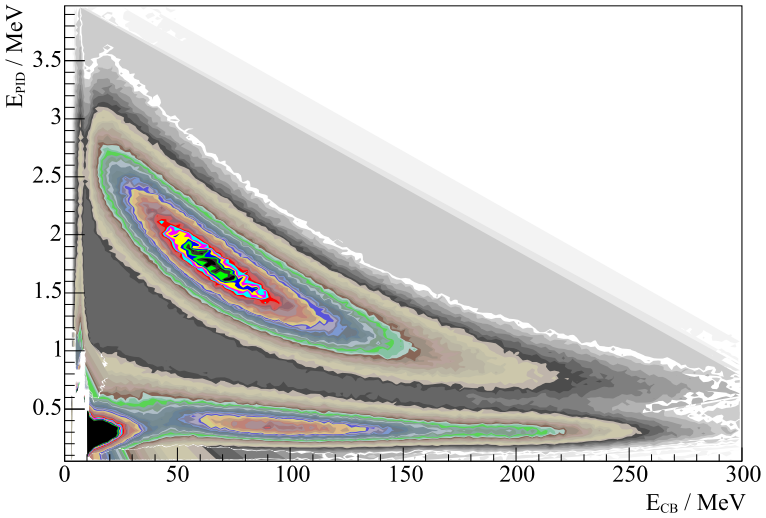

Figure 19: A typical $\Delta E/E$ plot from the Crystal Ball and the PID2 detector. The upper curved region is the proton locus, the lower region contains the pions and the peak towards the origin contains mostly electrons.

or two crystals, this is not so precise. Here the tracks of charged particles emitted within the angular and momentum acceptance of the CB detector will be reconstructed from the coordinates of point of intersections of the tracks with two coaxial cylindrical multiwire proportional chambers (MWPCs) with cathode strip readout. These MWPCs are similar to those installed inside the CB during the first round of MAMI-B runs [34]. The most significant difference is that all detector signals are taken at the upstream end of the MWPCs, minimizing the material required and facilitating particle detection in the forward polar region.
A mixture of argon (79.5%), ethane (30%) and freon-CF_4 (0.5%) is used as the filling gas. This mixture is a compromise between charge multiplication and localization requirements imposed by the ionizing particle tracks.
Within each chamber both the azimuthal and the longitudinal coordinates of the avalanche will be evaluated from the centroid of the charge distribution induced on the cathode strips. The location of the hit wires(s) will be used to resolve ambiguities which arise from the fact that each pair of inner and outer strip cross each other twice. The expected angular resolution (rms) will be $\sim 2^\circ$ in the polar emission angle θ and $\sim 3^\circ$ in the azimuthal emission angle ϕ.
The MWPCs have been recently installed inside the CB frame and their calibration using both cosmic rays and test beam data is currently underway.

A.4 TAPS Forward Wall

The TAPS forward wall is composed of 384 BaF_2 elements, each 25 cm in length (12 radiation lengths) and hexagonal in cross section, with a diameter of 59 mm. The front of every TAPS element is covered by a 5 mm thick plastic veto scintillator. The single counter time resolution is $\sigma_t = 0.2$ ns, the energy resolution can be described by $\Delta E/E = 0.018 + 0.008/E[\mathrm{GeV}]^{0.5}$ [33]. The angular resolution in the polar angle is better than 1°, and in the azimuthal angle it improves with increasing θ, being always better than $1/R$ radian, where R is the distance in centimeters from the central point of the TAPS wall surface to the point on the surface where the particle trajectory meets the detector. The TAPS readout was custom built for the beginning of the CB@MAMI program and is effected in such a way as to allow particle identification by Pulse Shape Analysis (PSA), Time Of Flight (TOF) and $\Delta E/E$ methods (using the energy deposit in the plastic scintillator to give ΔE). TAPS can also contribute to the CB multiplicity trigger

and is currrently divided into up to six sectors for this purpose. The two inner rings of 18 BaF_2 elements have been replaced recently by 72 $PbWO_4$ crystals each 20 cm in length (22 radiation lengths). The higher granularity improves the rate capability as well as the angular resolution. The crystals are operated at room temperature. The energy resolution for photons is similar to BaF_2 under these conditions [35].

References

[1] J.W.C. McNabb *et al.* (CLAS Collaboration), Phys. Rev. C **69**, 042201 (2004).

[2] R.G.T. Zegers *et al.*, Phys. Rev. Lett. **91**, 092001 (2003).

[3] S. Goers *et al.* (SAPHIR Collaboration), Phys. Lett. B **464**, 331 (1999).

[4] M.Q. Tran *et al.* (SAPHIR Collaboration), Phys. Lett. B **445**, 20 (1998).

[5] K. Tsukada *et al.*, Phys. Rev. C **78**, 014001 (2008).

[6] T. Feuster and U. Mosel, Phys. Rev. C **58**, 457 (1998).

[7] S. Capstick and W. Roberts, Phys. Rev. D **58**, 074011 (1998).

[8] S. Capstick, Phys. Rev. D **46**, 2864 (1992).

[9] J.J. Jones *et al.*, Phys. Rev. Lett. **26**, 860 (1971).

[10] D. Rebreyend *et al.*, Int. J. Mod. Phys. **A20**, 1554 (2005).

[11] V. Kuznetsov and M.V. Polyakov, JETP Lett. **88**, 347 (2008).

[12] C. Amsler *et al.* (Particle Data Group), *Review of Particle Physics*, Phys. Lett. B **667**, 1 (2008).

[13] L. Bertanza *et al.*, Phys. Rev. Lett. **8**, 332 (1962).

[14] T.M. Knasel *et al.*, Phys. Rev. D **11**, 1 (1975).

[15] T.O. Binford *et al.*, Phys. Rev. **183**, 1134 (1969).

[16] D.H. Saxon *et al.*, Nucl. Phys. **B162**, 522 (1980).

[17] O. Van Dyke *et al.*, Phys. Rev. Lett. **23**, 50 (1969).

[18] O.I. Dahl *et al.*, Phys. Rev. **163**, 1430 (1967).

[19] M. Ripani, Eur. Phys. J. A **19**, s01, 71 (2004).

[20] J.C. David,C. Fayard, G.-H. Lamot, and B. Saghai, Phys. Rev. C **53**, 2613 (1996); T. Mizutani, C. Fayard, G.-H. Lamot, and B. Baghai, Phys. Rev. C **58**, 75 (1998).

[21] T. Mart and C. Bennhold, Phys. Rev. C **61**, 012201 (2000); F.X. Lee, T. Mart, C. Bennhold, and L.E. Wright, Nucl. Phys. **A695**, 237 (2001).

[22] P. Bydžovský and M. Sotona, Nucl. Phys. **A754**, 243 (2005); P. Bydžovský, M. Sotona, O. Hashimoto, and T. Takahashi, nucl-th/0412035.

[23] R.A. Adelseck and B. Saghai, Phys. Rev. C **42**, 108 (1990).

[24] R.A. Williams, C.R. Ji, and S.R. Cotanch, Phys. Rev. C **46**, 1617 (1992).

[25] E. Munevar, B.L. Berman and P. Nadel-Turoński (CLAS Collaboration), AIP Conf. Proc. **947**, 146 (2007).

[26] T. Watanabe *et al.* Phys. Lett. B **651**, 269 (2007).

[27] R. Castelijns *et al.* (CBELSA/TAPS Collaboration), Eur. Phys. J. A **35**, 39 (2008).

[28] Sugat Vyankatesh Shende, Ph.D. thesis, Kernfysich Versneller Insititute, Rijksuniversiteit Groningen, Groningen (2007).

[29] R. Lawall *et al.* (SAPHIR Collaboration), Eur. Phys. J. A **24**, 275 (2005).

[30] J. C. McGeorge *et al.*, Eur. Phys. J. A **37**, 129 (2008).

[31] A. Reiter *et al.*, Eur. Phys. J. A **30**, 461 (2006).

[32] A. Thomas *et al.*, Nucl. Phys. **B79**, 591 (1999).

[33] S. Prakhov *et al.*, Phys. Rev. C **79**, 035204 (2009).

[34] G. Audit *et al.*, Nucl. Instr. Meth. A **301**, 473 (1991).

[35] R. Novotny *et al.*, Nucl. Instrum. Meth. A **486**, 131 (2002).